AIChE InterScience DISCOVER SOMETHING GREAT

MATERIALS, INTERFACES, AND ELECTROCHEMICAL PHENOMENA

Packing Structure of MPS SAMs and Its Influence on Oriented Deposition of SnO_2 Crystal Films

Jinli Zhang, Ming Zhang, Wei Li, and Yi Zhai
School of Chemical Engineering and Technology, Tianjin University, Tianjin 300072, P.R. China

DOI 10.1002/aic.11305
Published online September 12, 2007 in Wiley InterScience (www.interscience.wiley.com).

The (110) crystal plane of SnO_2 was found by X-ray diffraction, atomic force microscopy and X-ray photoelectron spectroscopy to grow preferentially in the direction of short-chain sulfonate self-assembled monolayer (SAM) formed from in situ oxidation of 3-mercaptopropyltrimethoxysilane (MPS) treated Si substrates. Molecular simulations were performed to study the optimal packing structure of MPS SAMs on Si (100) surface as well as its induced deposition mechanism to the SnO_2 crystal. Molecular mechanics calculations showed that the MPS molecules self-assembled on Si (100) surfaces with a coverage ratio of 50% and a zigzag-like packing pattern. Molecular dynamics calculations reflected that oxidation of the —SH of MPS contributed to uniform —SO_3H-terminated SAMs with narrower distribution of dihedral angles. Density functional theory calculations suggested the existence of strong interactions between the —SO_3H groups of SAMs and SnO_2 (110) plane, which was due to the structural and electrical match between the —SO_3H group and the unsaturated atoms on SnO_2 (110) plane. These results consistently confirmed that the ordered SAMs with —SO_3H terminal group are beneficial to the epitaxial growth of crystal SnO_2. © 2007 American Institute of Chemical Engineers *AIChE J*, 53: 2957–2967, 2007
Keywords: crystal growth, self-assembly, simulation, quantum mechanics, SnO_2 films

Introduction

Self-assembled monolayers (SAMs) of organic molecules provide a convenient way to tailor the properties of the surface and the interfaces of solid-state materials. Applications of SAMs have attracted attention in diverse areas including surface modification,[1] lubricant coatings,[2] chemical sensors/biosensors,[3–6] electrochemical studies,[7] immobilization of DNA,[8] and especially preparation of nanocrystal materials. For instance, crystalline SnO_2 film have been successfully prepared on substrates modified by long-chain SAMs such as octadecyltrimethoxysilane[9,10] and 1-thioacetato-16-(trichlorosily)hexadecane.[11] Highly oriented microrods of ZnO crystals were synthesized on Si wafers with the SAMs of $SiCl_3(CH_2)_{11}—O—C_6H_4—COOH$.[12] Calcite plane $(01\bar{1}2)$ was induced to grow under the orientation of 16-mercaptohexadecanoic acid SAMs.[13–15] Crystalline TiO_2 (anatase)thin films were deposited onto organic alkylsilane SAMs of 1-trifluoroacetato-16(trichlorosilyl) hexadecane and 1-thioacetate-16-(trichlorosilyl) hexadecane with —OH and —SO_3H terminal groups.[16,17]

So far, most investigations on the metal oxide film growth have concentrated on utilizing SAMs of long-chain molecules because short-chain molecules are considered to form self-assembled layers with poorly ordered structures. Ito et al.[18] studied the SAMs structure of two COOH-terminated alkanethiols [11-mercapto-undecanoic acid (MUA) and 6-mercapto-hexanoic acid (MHA)] on Au (111), and found the longer alkyl chain (MUA) formed a well-ordered monolayer, while the shorter-chain (MHA) formed a nonuniform film. In Nuzzo and coworker's research,[19] Fourier transform infrared

This article contains supplementary material available via the Internet at http://www.interscience.wiley.com/jpages/0001-1541/suppmat.

Correspondence concerning this article should be addressed to Dr. W. Li at liwei@tju.edu.cn.

spectroscopy results indicated that the longer chain alkanethiols $HS(CH_2)_nCH_3$ (n = 15, 17) form well-defined SAMs with crystalline-like conformations, and there is less conformational order present in the monolayers of short-chain (n = 7) molecules. Prathima et al.[20] compared the SAM of C8 and C18 alkanethiols on the Au (111) surface, and concluded that the SAMs of short-chain C8 alkanethiols had more defects than those of the long-chain C18 alkanethiols. However, no report was found to illuminate the effect of terminal groups on the packing structure of SAMs.

Micro-structures of SAMs are important to understand the interaction mechanism at deposition interfaces. Advanced experimental techniques have been used to characterize the structure of SAMs, such as Atomic Force Microscopy (AFM), Infrared Spectroscopy, contact angle goniometry, ellipsometry, X-ray Diffraction (XRD), X-ray Photoelectron Spectroscopy (XPS), and surface plasmon resonance.[18,21,22] More recently, computational simulations, including molecular mechanics (MM),[23,24] molecular dynamics (MD),[25] and quantum mechanics (QM)[26] calculations, have proven useful to explore detailed information of the SAMs structure, which can be difficult to measure by experimental techniques. For example, Zhang et al.[25] studied the packing structures of C18 alkyl SAMs on the Si (111) using MD simulation, and found that C18 alkyl groups arranged uniformly with a tilt angle about 28°.

Tin oxide (SnO_2) is a type of wide band-gap n-type semiconductor that is widely used in dye-sensitized solar cells,[27] Li-ion batteries,[28,29] transparent conductive electrodes,[30] and gas sensors.[31,32] Although many groups have grown the SnO_2 films on SAMs-coated substrates through liquid phase deposition[33,34] or liquid flow deposition,[35] the influence of self-assembled layers on the subsequent deposition of tin oxide remains elusive, especially for the short alkoxyl-chain SAMs. In a previous work, we have successfully synthesized compact crystalline SnO_2 films on substrates coated with self-assembled layers of a short-chain alkylsilane molecule, 3-mercaptopropyltrimethoxysilane (MPS), and found that the kind of terminal group of MPS-SAMs greatly influenced the morphology of deposited SnO_2 films.[36] However, it is not well understood yet how the packing structure of MPS-SAMs affects the epitaxial growth of metal oxide crystals.

In this article, we investigated the structure of the short-chain MPS SAMs as well as its influence on the oriented growth of SnO_2 crystal films using experimental characterizations and computational calculations. The distinctness of SnO_2 crystals precipitated homogeneously in precursor solutions was compared with those deposited on the SO_3H-terminated MPS SAMs. According to experimental results, simulation models were established and then MM and MD simulations were performed to study the optimal packing structures of MPS SAMs on a Si (100) plane. The radial distribution of sulfur atoms and dihedral angles variations were investigated using dynamic simulations before and after oxidizing the terminal —SH groups of MPS. Finally, DFT calculations were adopted to study the interaction of the SO_3H-terminated monolayer and SnO_2 crystal. Both the experimental and the simulation results revealed the main reason behind the observation that the short alkoxyl-chain SO_3H-terminated MPS-SAMs influences the SnO_2 crystal orientation during the deposition process. This work provides us with a potential route to adjust crystal growth on substrates, which has promising applications in the design and production of desirable semiconductor films and catalysts.

Experimental and Modeling Methods

Deposition of SnO_2 films on MPS-coated substrates

The square silicon wafers (1 cm × 1 cm) were cleaned ultrasonically in ethanol and in deionized water for 20 min respectively, to remove possible contaminants on the surfaces. Then the wafer pieces were immersed in a freshly prepared "piranha" solution of 1:3 (v/v) mixture of 30% H_2O_2 and concentrated sulfuric acid at 80°C for 30 min to become oxidated and hydroxylated. Self-assembled layers of MPS were formed on the hydroxylated substrates at room temperature through dipping the clean wafers into 5 mM MPS cyclohexane solution. Then the MPS-coated substrates were treated in a mixture solution of H_2O_2 and acetic acid, to oxidize the —SH groups of MPS layers into the desired $-SO_3H$ groups. The sulfonic functionalized substrates were immersed into the fresh precursor solution of 2 mM $SnCl_4$ and 0.4 M HCl to deposit SnO_2 films. The detailed procedure of the film deposition was reported in the previous report.[36]

The zeta potential of colloidal particles was measured with a Malvern ZetaSizer 3000HSA (Malvern Instruments). The particle morphology was observed using a NanoScope IIIa MultiMode Scanning Probe Microscope (Digital Instruments) in the tapping mode. All the AFM images were recorded with the tip scanning from the bottom of the imaged area in air at room temperature. The deposited tin oxide films were characterized using XRD and XPS. The powder X-ray diffraction patterns of oxide films were obtained for phase identification using a D/MAX II-2038 diffractometer (Philips) with a Cu Kα radiation at 40 kV. The elemental composition of the films was determined using XPS (PHI 1600 ESCA System). XPS measurements were operated at a power level of 300 W with an Mg Kα X-ray source. Electron binding energies were calibrated against the alkyl C 1s emission peak at 284.6 eV.

Modeling methods

All the calculations including QM, MM, and MD studies were performed with a DELL workstation using the Materials Studio package (version 3.1) from Accelrys.[37] The QM calculations were based on the Dmol3 module, and the MM&MD simulations were performed using the Discover module with the COMPASS[38] force field. Two points were the focus of this work, one was the SAMs structure of short chain molecules (MPS) on a hydroxyl-terminated Si surface at a molecular level; the other was the selective deposition mechanism of these MPS SAMs to the SnO_2 crystal films.

The MPS SAMs model and simulation methods

The Si (100) surface is the most important reconstructed surface.[39,40] In all kinds of Si (100) reconstruction surfaces, the 2 × 1 reconstruction is the most stable structure.[41–43] In our simulation, we created the Si (100) 2 × 1 reconstructed surface including four layers of silicon atoms as the

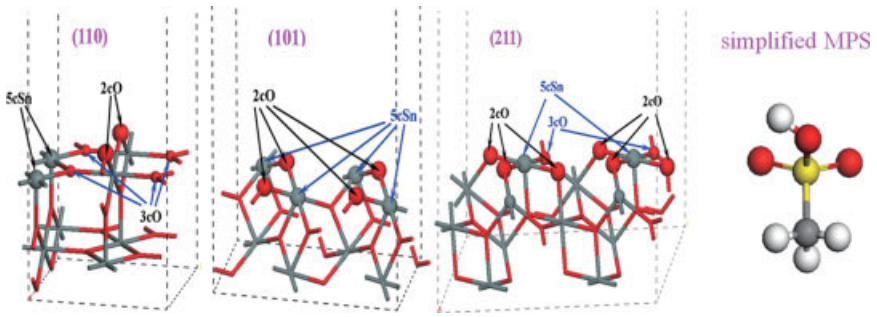

Figure 1. The structure of SnO_2 crystal planes (110), (101), (211) and the simplified MPS.

[Color figure can be viewed in the online issue, which is available at www.interscience.wiley.com.]

substrate. The bottom two layers of silicon atoms were fixed at their bulk crystal positions during all the calculations. The silicon atoms in the upmost layers were initially terminated with hydroxyl groups to describe the starting surface treated by the first step in the experimental process.[21] And then a vacuum slab of 30 Å was added onto the surface to avoid the interaction between different slabs. Thus the basic Si (100) 2 × 1 cell has a dimension of 3.08 Å × 7.68 Å × 35.00 Å. This (2 × 1) unit cell was then extended in two dimensions via the use of periodic boundary conditions to generate other simulation cells such as (2 × 2), (2 × 4), (4 × 4), and (16 × 16). MPS molecule was optimized using MM calculation for nearly 2000 steps, and then replaced the surface hydroxyl groups at the appropriate positions via a Si—O linkage, to obtain the models used to describe the modified surfaces. The thiol groups (—SH) in the SAMs were subsequently replaced by the sulfonic group ($—SO_3H$) to describe the oxidized surfaces onto which metal oxide films were deposited. The resulting surfaces were subjected to a MM optimization with the "smart minimizer" method, which consisted of three cascade-minimized methods (Steepest Descent, Conjugate Gradient, Newton). An "ultra-fine" convergence criterion (10^{-5} kcal/mol) was adopted in the simulation with Ewald summation for van der Waals (vdW) and electrostratic (Coulomb) nonbond calculations.

The optimal packing structure of MPS on Si (100) surface was obtained through comparing the average packing energy per chain of all different structures. The average packing energy per chain of the MPS molecule (E_{ave}) was calculated using the following equation

$$E_{ave} = (E_{total} - E_{Si})/N \quad (1)$$

where E_{total} represents the total energy of the Si (100) surface binding the MPS molecule, E_{Si} is the energy of the hydroxyl-terminated Si (100) surface, and N is the number of substituted MPS molecules. A lower E_{ave} value corresponds to a stable packing structure.

Then MD simulations were further performed on both energy-minimized systems with —SH and $—SO_3H$ groups using an NVT ensemble. Three-dimensional periodic boundary conditions (PBC) were applied in the MD simulation. The MD temperature was set at 298 K, which was controlled by the Berendsen et al.[44] thermostat. The step time was 1 fs. The equilibration time was 100 ps, The resulting trajectory files were then viewed and analyzed by a variety of properties such as the angle, dihedral, and the distribution of functional groups on the surface.

The crystal deposition model and simulation methods

To explore the reason that MPS SAMs influence the crystal growth of SnO_2, we studied the interactions between the SAMs and SnO_2 crystal planes that exhibited major peaks in XRD patterns, such as the planes (110), (101), (211). The surface atoms located in these three different crystal planes can be classified according to their coordinate behavior. The coordinately unsaturated atoms, such as fivefold-coordinated Sn (5cSn) and twofold-coordinated O (2cO), provide most of the promising sites interacting with MPS molecules. On the other hand, the coordinately saturated atoms involving 6cSn and 3cO are relatively inert in terms of interacting with MPS molecules. A simplified model was adopted to simulate the oxidized MPS molecule, including a single methyl group (CH_3) and the function group ($—SO_3H$) as shown in Figure 1. In the following section, this simplified model was named as MPS-mod. Except for this CH_3SO_3H model, the other simplified model, $CH_3CH_2SO_3H$, was also considered in this work.

The Perdew–Burke–Enzerhof (PBE) function[45] based on the generalized gradient approximation (GGA) method with double numerical plus d-functions (DND) base was used, and the all electron method was chosen to treat the nuclear interactions. The energy convergence was set to 1×10^{-6} Ha (1 Ha = 2625.5 kJ/mol). The binding energy ΔE was defined as below to depict the binding probability and stability between the MPS-mod and SnO_2 crystal planes,

$$\Delta E = E(\text{total}) - E(SnO_2) - E(\text{MPS} - \text{mod}) \quad (2)$$

where E(total) was the energy of the complex including MPS-mod and SnO_2 plane, $E(SnO_2)$ and E(MPS-mod) were the sole energy of SnO_2 crystal plane and the MPS molecule model, respectively. A negative value of ΔE suggests a stable structure of the complex as well as preferable interactions between the MPS-mod and the crystal plane.

Results and Discussion

Crystal orientation of heterogeneous deposited films

Hydrolysis reaction of $SnCl_4$ resulted in the formation of colloidal particles, of which zeta potential were measured as

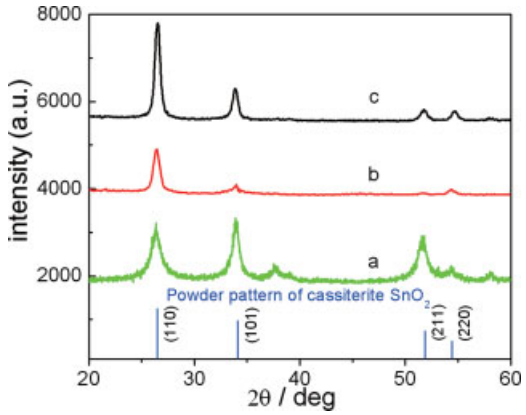

Figure 2. X-ray diffraction patterns.

(a) Homogeneous precipitate in a precursor solution at 80°C for 12 h, and heterogeneous deposited film on MPS-coated substrates with the immersion time of (b) 8 h and (c) 24 h. [Color figure can be viewed in the online issue, which is available at www.interscience.wiley.com.]

a function of reactive time. The zeta potential was 5.02 mV at 0.5 h and increased with time (as shown in Figure S1 of Supporting Information). The fresh precursor solution containing 2 mM $SnCl_4$ and 0.4 M HCl had a pH value about 0.82 and kept clear in the first 4 h at 80°C, which suggested a low hydrolysis rate of this solution. AFM images reflected that small amount of colloidal particles existed in the fresh solution with the largest diameter about 16 nm, and the amount of particle increased and the largest size was larger as 70 nm at 4 h. When the time was up to 12 h, the aggregate of particles were observed (as shown in Figure S2 of Supporting Information), which were filtrated and washed so as to analyze its crystal structure. These particles separated from the solution were named as the homogeneous precipitates to differentiate them from the film deposited onto the substrate.

Figure 2 showed XRD patterns of homogeneous precipitates and the films deposited on the $-SO_3H$-terminated MPS SAMs with a immersion time of 8 and 24 h, which are typical of crystalline SnO_2 (cassiterite). Comparing these XRD patterns, it is intriguing to find that the crystal orientation of the films deposited on the functionalized substrates is obviously different from that precipitated homogeneously in the precursor solution. It is suggested that during the heterogeneous deposition the (110) crystal plane of SnO_2 preferentially grew on the MPS-coated substrates, while the growth of the (101) and (211) planes appeared to be constrained. SEM image of the deposited SnO_2 film was shown in Figure S3 of the Supporting Information, which displayed the uniformly deposited SnO_2 films. These results reflected the fact that the $-SO_3H$ terminal of short-chain MPS SAMs play an important role in the epitaxial growth of the SnO_2 crystals. In previous reports,[9–11] SnO_2 films were synthesized on the long-chain alkylsilane SAMs, however, they did not report the influence of the SAMs on the crystal orientation.

Understand the packing structure of MPS SAMs and interactions between this SAMs and the deposited tin oxide is fundamental to not only the deposition of desirable crystalline semiconductor films but also for the adjustment of catalyst activities. Senkevich et al.[46] suggested two potential pathways for MPS growth on the surface, one is the so-called "lying pathway" in which the two terminals of the MPS molecules kept almost the same distance to the substrate, and the other is the "vertical pathway" in which the trimethoxy terminal of MPS located close to the substrate so that the molecule was approximately perpendicular to the substrate. The high-resolution XPS spectra were compared with various take-off angles for the substrate treated in 5 mM MPS solution (as shown in Figure 3). Intensity of Si2p obviously increased as the take-off angle of the X-ray beam changed from 10° to 90°, which suggested that the probed depth increased at larger take-off angle. Meanwhile the intensity of C 1s decreased significantly and the intensity of S 2s only slightly decreased as the take-off angle increased. The atomic concentration of C 1s and S 2p, characterized by XPS spectra, was 10.7% and 2.6% respectively at the 45° take-off angle.[36] According to the XPS spectral variations along with the take-off angles and the atomic concentration distribution of element species, it is reasonable for the MPS molecules to adopt the "vertical pathway" on the substrate, i.e., its trimethoxy group connected directly with the substrate surfaces while its thiol group located beyond the surfaces.

Additionally we investigated the possibility of any crosslinking between MPS molecules, e.g. Si—O—Si bonds forming between two MPS molecules. Assuming a crosslinking of Si—O—Si bond forming between two MPS molecules at the initial state, the —SH terminal groups of MPS molecules run in the opposite direction after the optimization. As shown in Figure S4 (see the supporting information), the distance between sulfur atoms of —SH groups increased from 5.2 to 11.3 Å if there existed a Si—O—Si bond. The departure of the terminal groups was due to the fact that the covalent bond lengths of Si—O—Si are shorter than van der Waal diameters of C and H atoms in the alkyl chains.[47] As shown in Figure 8, the radial distribution of sulfur atom in the SH-terminated SAMs is around 4.75 Å. The large difference of two adjacent sulfur atoms' distance suggest against the existence of crosslinking of Si—O—Si bond between two MPS molecules. Therefore, in the following simulation studies the model of MPS SAMs was established according to the "vertical pathway" location of MPS without cross-linking on the substrate.

Molecular mechanics calculations of the self-assembled MPS monolayer

The PBC model of MPS on Si (100) surface was established for the DFT and MM calculations (shown in Figure 4). Firstly the accuracy of the COMPASS force field was validated for this studied system. Table 1 lists the optimized geometric parameters of the PBC model obtained by using DFT, PCFF, and COMPASS. It is shown that no significant variations were resulted from using different DFT functions (PW91, BLYP). Comparing the geometric parameters optimized using COMPASS and PCFF, it is obvious that the COMPASS force field is superior over the PCFF for providing accurate predictions of geometries, as the bond lengths of C4—Si5, Si5—O6, and O6—Si7 obtained using COMPASS were 1.89, 1.64, and 1.67 Å respectively, which is in good agreement with the related DFT values. The bonding angle

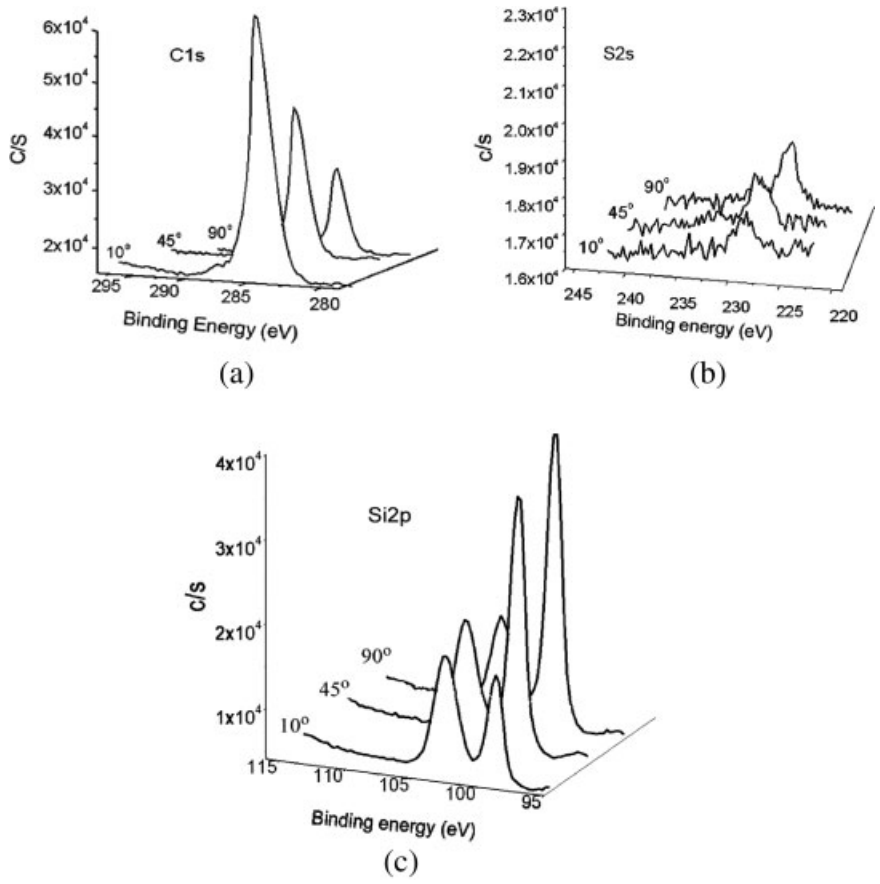

Figure 3. High-resolution XPS spectra of C 1s: (a), S 2s (b) and Si 2p (c) with various take-off angles for the substrate treated in 0.005 M MPS for 3 h.

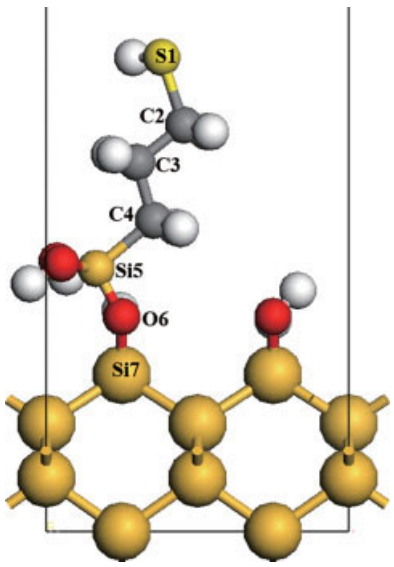

Figure 4. The 2 × 2 sized PBC model of MPS on Si (100) surface for the DFT and MM calculations.

Yellow is Si, red is O, white is H, gray is C. [Color figure can be viewed in the online issue, which is available at www.interscience.wiley.com.]

$\angle Si_5—O_6—Si_7$ (152.5°) from COMPASS calculations was also close to the DFT results. In contrast, the PCFF calculation predict a bonding angle $\angle Si_5—O_6—Si_7$ of 130.6° instead. Thus, the COMPASS force field was adopted to simulate this model system.

Surface coverage ratio and coverage pattern are two important factors to be considered in the SAM system. For a specific surface coverage ratio except for the full coverage of

Table 1. Bond Lengths and Bond Angles of the Model of MPS Adsorbed on Si (100) Surface, Calculated Using DFT with Different Function and MM with PCFF and COMPASS Force Field, Respectively

	DFT		MM	
Optimized Geometries	PW91	BLYP	PCFF	COMPASS
S1—C2, Å	1.84	1.86	1.83	1.83
S1—C2—C3, deg	114.1	114.7	110.4	114.1
C2—C3, Å	1.53	1.54	1.53	1.53
C2—C3—C4, deg	113.1	112.5	113.3	112.7
C3—C4, Å	1.54	1.56	1.53	1.54
C3—C4—Si5, deg	112.3	113.8	111.3	113.3
C4—Si5, Å	1.87	1.88	1.90	1.89
C4—Si5—O6, deg	113.0	112.6	113.2	112.1
Si5—O6, Å	1.64	1.65	1.66	1.64
Si5—O6—Si7, deg	157.3	156.8	130.6	152.5
O6—Si7, Å	1.67	1.69	1.61	1.67

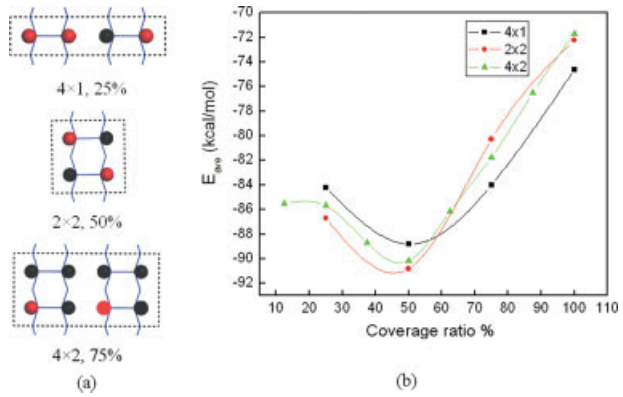

Figure 5. (a) Three different molecular patterns placed on the Si (100) surface with the simulation cells of 4 × 1, 2 × 2, and 4 × 2; red balls represent unsubstituted site, black balls represent substituted site; (b) average packing energy per chain for MPS adsorption on Si (100) surface with different coverage ratios.

[Color figure can be viewed in the online issue, which is available at www.interscience.wiley.com.]

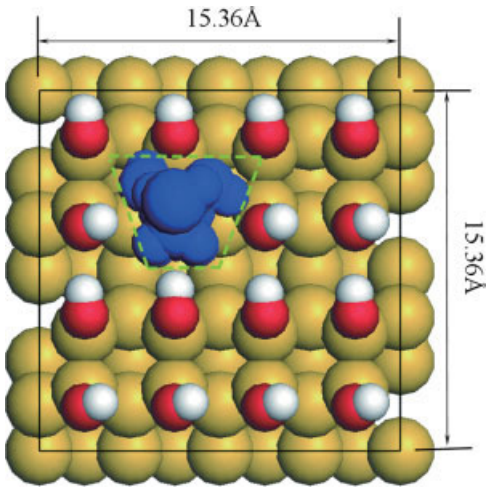

Figure 6. The sketch of one MPS molecule located perpendicularly on Si (100) 4 × 4 surface.

[Color figure can be viewed in the online issue, which is available at www.interscience.wiley.com.]

100%, different coverage patterns could be formed when the MPS molecules substituted hydroxyl groups on the surface. A number of different molecular patterns were placed on the Si (100) surface to generate initial structures at the specified surface coverage ratio ranging from 12 to 100%. MM simulations were performed on these structures of different substitution patterns so as to compare the corresponding molecular packing energies per chain. Figure 5a depicts the representative simulation cells of 4 × 1, 2 × 2, and 4 × 2 with different substitution patterns. Figure 5b shows the average packing energies per chain (E_{ave}) as a function of the surface coverage ratio of MPS using different simulation cells. As shown in Figure 5b, the lowest E_{ave} value located around the point with 50% coverage ratio for all these substitution patterns.

We estimated the theoretical maximum coverage ratio of MPS molecules bound to a Si (100) 4 × 4 surface by using the van der Waals volume calculations. Figure 6 indicates a sketch of one MPS molecule located perpendicularly on a Si (100) 4 × 4 surface. The projected largest section of the MPS molecule is highlighted by a green dashed-lined trapezium, and the boundary of the Si surface is marked by a black-lined square. The trapezium area approximates 26 $Å^2$, while the square area is 236 $Å^2$ for Si (100) 4 × 4 surface. Accordingly, nine perpendicular molecules of MPS are enough to cover the entire Si (100) 4 × 4 surface, although this surface could provide sixteen potential binding sites. Thus the maximum coverage ratio of MPS is estimated to be 56%. In view of the average packing energies shown in Figure 5b, the coverage ratio was fixed at 50% in the following calculations.

To analyze the optimal packing pattern of the MPS monolayer on a Si (100) surface, a number of different cells were calculated with various molecular packing patterns at the specified 50% coverage ratio by using a MM minimization method. As in previous studies,[23–26] two types of surface packing patterns, i.e., the linear pattern and the zigzag pattern, were investigated in the present study. Figure 7 depicts the simulation cells, in which the cells of (a), (c), (e), and (g) represent the linear packing pattern, while the cells

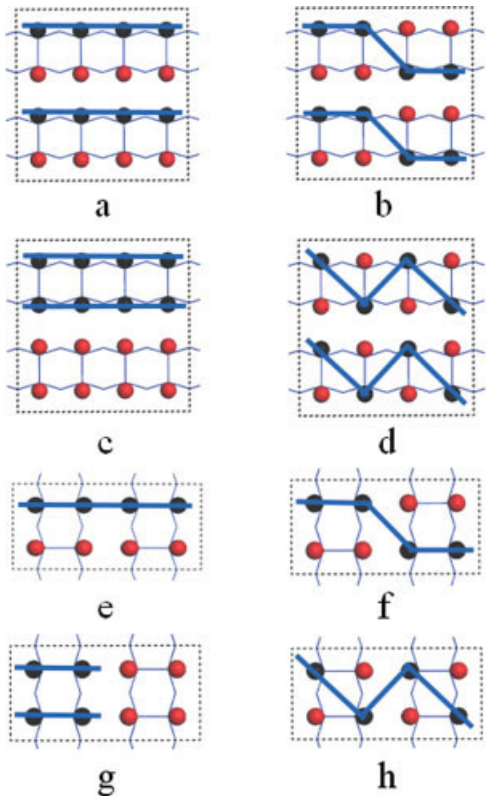

Figure 7. Different simulation cells with various packing pattern at 50% coverage ratio.

The red balls represent unsubstituted sites, and the black balls represent substituted sites. [Color figure can be viewed in the online issue, which is available at www.interscience.wiley.com.]

Table 2. Average Packing Energy per MPS Molecule on Si (100) Surface for Different Simulation Cells at 50% Coverage Ratio

Pattern	Simulation Cell	E_{ave}, kcal/mol
a	4 × 4	−85.4106
b	4 × 4	−89.0887
c	4 × 4	−79.8274
d	4 × 4	−89.6948
e	2 × 4	−86.4878
f	2 × 4	−88.3074
g	2 × 4	−83.8929
h	2 × 4	−90.1833

of (b), (d), (f), (h) are the zigzag patterns. Table 2 lists the values of the average packing energy per MPS molecule (E_{ave}) for each of these simulation cells. Compared to cells (a), (c), (e), and (g), the values of E_{ave} of cells (b), (d), (f) and (h) are much lower, with the (h) structure has the lowest E_{ave}, which indicated that the zigzag packing pattern is preferable for a MPS monolayer on Si (100). Comparing cells with the same packing pattern but different size, e.g., (a) and (e), (d) and (h), it is noted that the value of E_{ave} slightly depends on the simulation cell size. Such kind of size-dependent behavior was also reported for the packing of long alkyl molecule C18 assembled on Si (111) surface.[18] As far as the small difference between two different zigzag patterns is considered, for instance, (b) or (f) versus (d) or (h), it is possible that these two conformations may coexist in real reactive conditions. In the following simulations, the zigzag packing pattern (h) was adopted as the primary structure.

Molecular dynamics calculations of the MPS monolayer packing structures

Our experimental results indicated that original MPS SAMs with the terminal group of —SH was not beneficial to form uniformly deposited SnO_2 films on the substrate. However, upon the —SH group was transferred into —SO_3H group after being oxidized, the uniform SnO_2 films preferably grew at the interface. Therefore it would be very interesting to study the packing structure of MPS monolayer with the terminal group of —SH and —SO_3H. Toward the goal, we carried out MD simulations on the Si (100) 16 × 16 surface, the extended cell with the packing pattern (h). Such a cell consists of nearly 4000 atoms including 128 MPS molecules and four layers of Si atoms.

Figure 8 showed the radial distribution of sulfur atoms of the terminal groups of MPS before and after oxidation. The modal distribution of sulfur atoms in the SH-terminated SAMs was located around 4.75 Å, while the main radial distribution peak of sulfur atoms after oxidation shifted to 5.25 Å with higher intensity and narrower width. In addition, there exist a shoulder at 7.45 Å and a small peak at 11.25 Å for sulfur atoms in the SO_3H-terminated SAMs. These results suggest that the sulfur atoms in the MPS-SAMs exhibit intermediate-ranged order (up to 1.1 nm) after oxidation.

Figure 9 displays the detailed molecular packing structure of the MPS-SAMs after 100 ps dynamic simulation at 298 K. Both the top and the side view of the 16 × 16 surface before and after oxidation indicate that the distance among adjacent sulfur atoms and their tilt angle tend to be more orderly in SO_3H-terminated SAMs than those in SH-terminated SAMs. It is worthwhile to mention that the distributed sites of sulfur atoms in SO_3H-terminated SAMs consists of an approximate square array with each side of length about 5.2 Å, which can be attributed to the main peak at 5.25 Å shown in Figure 8. Moreover, the diagonal distance of the sulfur atom square is in accordance with the shoulder peak at 7.45 Å in Figure 8, and the double length of one square line is close to the value of 11.25 Å.

The distribution of dihedral angles in the assembled monolayer further revealed the more ordered structure of SO_3H-terminated SAMs, compared with that of SH-terminated SAMs. Figure 10a suggests that the dihedral angle $C_4Si_5O_6Si_7$ of the thiol-terminated MPS monolayer, closest to the substrate surface, has a wide distribution ranging from −100 to 100° with 0° as the median. Three other dihedrals also show a similar three-peak distribution; the only distinction is that the intensity of the middle peak becomes higher as the dihedral goes beyond the surface. The fluctuant dihedral angles in Figure 10a suggested a poorly ordered monolayer of thiol-terminated MPS, which is consistent with a common conclusion from previous findings that short-chain silanes can not form ordered SAMs; for instance, short-chain alkanethiol (C = 7) showed the disordered SAMs[48,49] and the short-chain molecule 6-mercapto-hexanoic acid resulted in non-uniform SAMs.[20]

Upon oxidation of the terminal groups of MPS SAMs into —SO_3H groups, the dihedral angles of the monolayer established a narrower distribution (Figure 10b). Not only the outmost dihedral $S_1C_2C_3C_4$ tends to be lumped around 0°, but also the bottom $C_4Si_5O_6Si_7$ reduced to a double-peaked distribution. Apparently, oxidation of the thiol group caused terminal atoms of the monolayer to rearrange uniformly even though the —SH terminated MPS SAMs were not well-

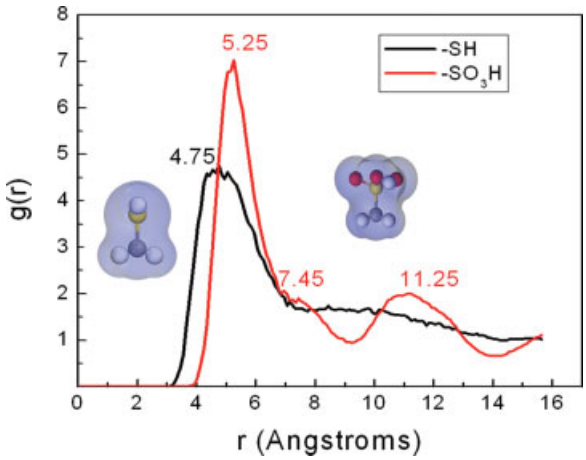

Figure 8. Radial distribution functions of sulfur atoms on the Si (100) 16 × 16 surface for 50 ps dynamic simulation.

The black line is corresponding to the thiol group, and the red line is to the sulfonate group. [Color figure can be viewed in the online issue, which is available at www.interscience.wiley.com.]

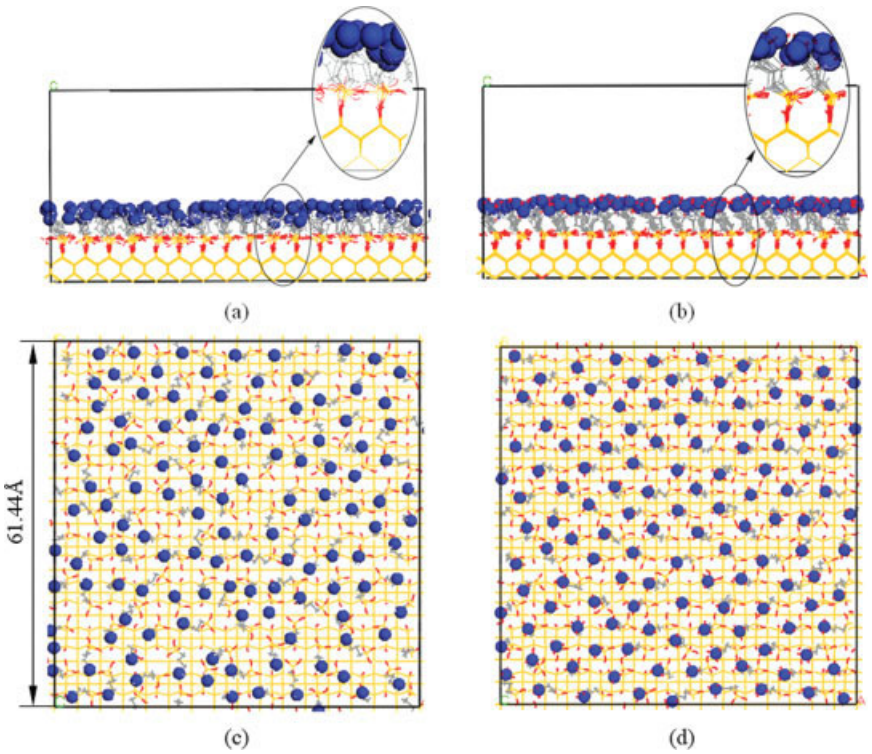

Figure 9. Packing structures of sulfur atoms on Si (100) 16 × 16 surface at 50% coverage ratio after 100 ps dynamic simulation.

(a) —SH, top view; (c) —SH, side view; (b) —SO_3H, top view; (d) —SO_3H, side view. The blue balls are sulfur atoms of the functional group, —SH or —SO_3H. Other atoms are shown using the stick model, the yellow is the silicon substrate, the red is oxygen, and the gray is carbon atom. [Color figure can be viewed in the online issue, which is available at www.interscience.wiley.com.]

ordered initially. It is the steric hindrance effect of the —SO_3H groups that constrains an arbitrary distribution of terminal atoms, consequently the order fashion of the SO_3H-terminated SAMs induces the formation of uniform SnO_2 films at the interface.

DFT calculations for interfacial interactions

To explore the main reason behind SAMs' influence on the crystal orientation during the deposition process, we adopted the DFT calculation method to study the interaction of the sulphonic-terminated monolayer with a SnO_2 crystal. A simplified self-assembled molecular model (MPS-mod) is comprised of one sulphonic group (—SO_3H) and one methyl group (—CH_3). The interactions of these two functional groups with major SnO_2 crystal planes, such as (110) (101) (211), were investigated using the PBE function based on the GGA method. The binding energy was calculated to discriminate the interactions of the SAM with different crystal planes.[50,51]

Table 3 showed the binding energies between the sulphonic group (—SO_3H) of the MPS-mod and three SnO_2 crystal planes. The binding energies of MPS-mod with SnO_2 (110) and (101) planes are negative, and the absolute value of ΔE on (110) plane is more than twice that on (101) plane. In combination with the XRD patterns characterization shown in Figure 2, the DFT calculations reasonably illuminate the facilitating effect of SO_3H-terminated SAMs on the SnO_2 (110) plane. The positive binding energy on plane (211) suggests an obstructive effect of the —SO_3H group on the growth of SnO_2 (211) plane.

Further calculations were performed to study potential interactions between the —CH_3 groups of the MPS-mod and the major SnO_2 planes. As illustrated in Figure 11, the binding energies are positive for all three SnO_2 planes approaching to the —CH_3 terminal. These results confirm that SnO_2 planes prefer interactions with the —SO_3H group to the —CH_3 group, which is in accordance with Supothina et al.'s report, i.e., discontinuous SnO_2 films formed on methyl-functionalized SAMs.[52]

To establish validity of the above findings using MPS-mod (CH_3SO_3H), another MPS molecular model ($CH_3CH_2SO_3H$) was also adopted in our work and the interactions between the modified MPS model, $CH_3CH_2SO_3H$, and SnO_2 planes were also calculated. As shown in Figure 11, $CH_3CH_2SO_3H$ showed the interaction with selected SnO_2 planes that was similar to that of the CH_3SO_3H model. The interactions between $CH_3CH_2SO_3H$ and three SnO_2 planes through —SO_3H terminal group are obviously stronger than through —CH_3 group. And the strongest binding also occurred between the SnO_2 plane (110) and —SO_3H group. These results verified that the established simple model (CH_3SO_3H) of MPS molecule is accurate enough to describe the interaction between the MPS-SAMs and SnO_2 planes.

Figure 12 showed the structure of one MPS-mod adsorbed on the SnO_2 plane (110) via the —SO_3H terminal before and

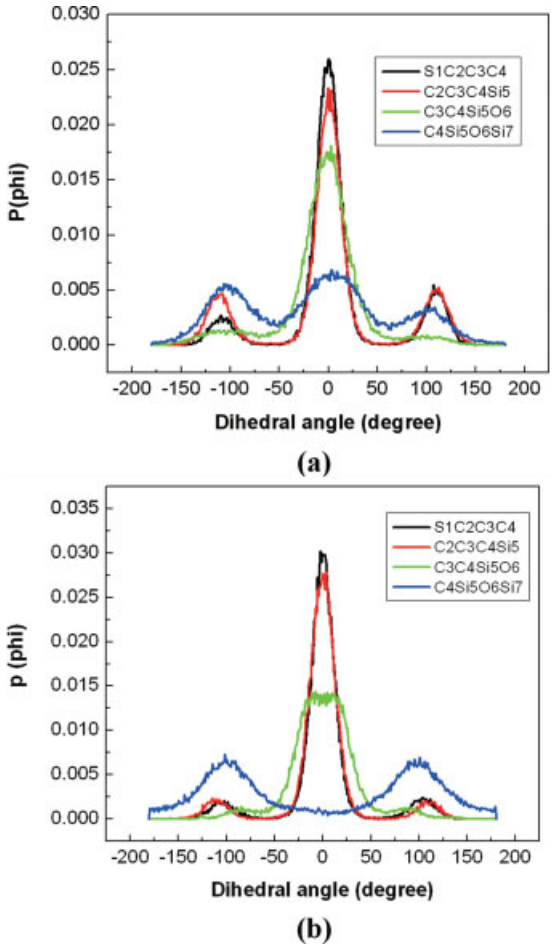

Figure 10. The distribution of torsion ($S_1C_2C_3C_4$, $C_2C_3C_4Si_5$, $C_3C_4Si_5O_6$, $C_4Si_5O_6Si_7$) in a 100 ps equilibrium dynamics.

(a) —SH group, (b) —SO_3H group. [Color figure can be viewed in the online issue, which is available at www.interscience.wiley.com.]

after the optimization. The initial state of the MPS-mod was perpendicular to the SnO_2 (110), with the sulfur atom located beyond the center of two 2c oxygen and two 5c tin atoms of the SnO_2. After energy minimization, the position of the MPS-mod not only shifted in the horizontal direction but also tilted about 45° in the vertical direction. Two oxygen atoms (O2,O3) of the —SO_3H group shifted from the center to the top of two 5c Sn atoms (Sn2, Sn3) and hydrogen atom (H1) of the —SO_3H moved to the top of the 2c oxygen atom (O1) in the SnO_2 (110) plane. As shown by the dashed triangle in Figure 12d, the projected area of atoms H1, O2, and

Table 3. The Binding Energy Between the —SO_3H Group and Three SnO_2 Crystal Planes

	(110)	(101)	(211)
E (total)	−50067.403	−50067.152	−74768.385
E (SnO_2)	−49403.214	−49403.029	−74104.459
E (MPS-mod)	−664.084	−664.084	−664.084
ΔE (Ha)	−0.106	−0.040	0.046
ΔE (KJ/mol)	−277.516	−102.908	98.635

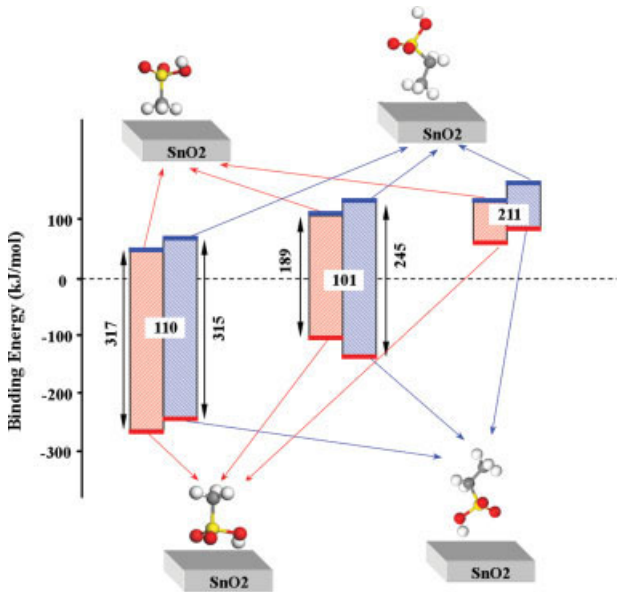

Figure 11. Potential energy diagram for the adsorption of CH_3SO_3H and $CH_3CH_2SO_3H$ on SnO_2 planes (110), (101), (211).

The red lines indicate the adsorption of —SO_3H group, and the blue lines are due to —CH_3 group. [Color figure can be viewed in the online issue, which is available at www.interscience.wiley.com.]

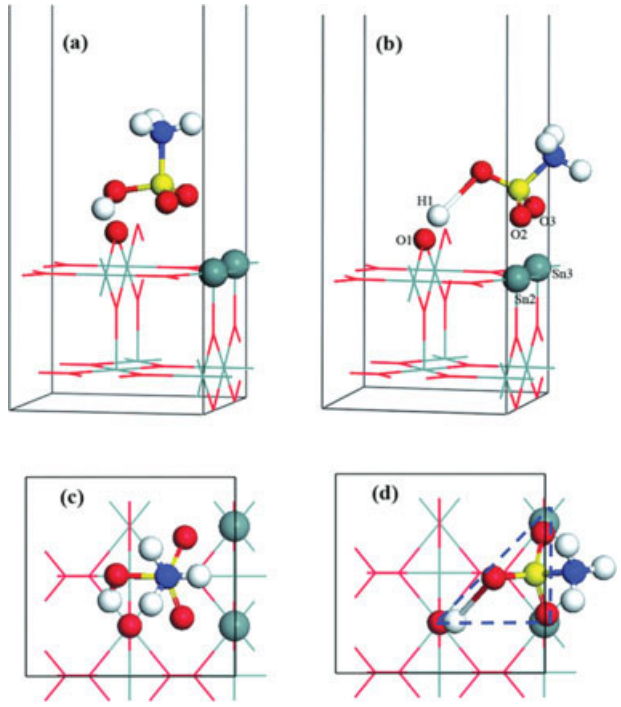

Figure 12. Adsorbed structures of CH_3SO_3H on SnO_2 plane (110).

Side view [(a), (b)] and the top view [(c), (d)]. (a) and (c) correspond to the initial structure, (b) and (d) are the optimized structure. Atom O is denoted as the red color, atom H is white, atom Sn is gray and atom C is blue. [Color figure can be viewed in the online issue, which is available at www.interscience.wiley.com.]

Table 4. Mulliken Charges of the Key Atoms in the Adsorption System of CH_3SO_3H on SnO_2 plane (110)

	Initial (*e*)	Optimized (*e*)	Δ*e*
H1	0.488	0.573	0.085
O2	−0.408	−0.559	−0.151
O3	−0.381	−0.557	−0.176
O1	−0.989	−1.075	−0.086
Sn2	2.035	2.111	0.076
Sn3	2.035	2.186	0.151
S	0.728	0.866	0.138

O3 in the $-SO_3H$ group was entirely overlapped with the area of atoms O2, Sn2, and Sn3 in the bottom SnO_2 (110) plane. Figure 12b indicates that the O—H bond length of the hydroxyl in the $-SO_3H$ group increased to 2.353 Å, while the distance between atom H1 in the $-SO_3H$ group and atom O1 in the SnO_2 (110) was as close as 0.980 Å. Furthermore the distance between atom O2 and atom Sn2 was 2.197 Å, and it was 2.223 Å for atom O3 and atom Sn3. Compared with the ionic bond length of Sn—O (2.054 Å) in bulk,[53] it is suggested that atoms H1, O2, and O3 in the $-SO_3H$ group interact strongly with the (110) plane of SnO_2, while atom H1 interacts weakly with the oxygen atom of the hydroxyl in the $-SO_3H$ group. Table 4 showed the Mulliken charge transfer for the atoms involved in the above three major interacting pairs, i.e., H1—O1, O2—Sn2, and O3—Sn3. The increased charge of H1 (0.085*e*) is nearly equal to the lost charge of O1 (−0.086*e*). For two other pairs (O2—Sn2, O3—Sn3), the charge transfer are not so simple as that of H1—O1 because the sulfur atom of $-SO_3H$ group also influences the charge transfer of atoms O2 and O3.

Conclusions

Experimental results indicated that crystal SnO_2 films epitaxially grew at the interface modified by the short-chain sulfonate terminated MPS-SAMs without calcination. Systematic molecular simulations including molecular mechanics, molecular dynamics and quantum mechanics-DFT methods disclosed that the SO_3H-terminated short-chain MPS can self-assemble into relatively ordered monolayer that plays a dominant role in adjusting the crystal orientation of the deposited SnO_2 film at the interfaces.

Molecular mechanics calculations showed that the optimal packing structure of MPS on Si (100) surface had a coverage ratio of 50% and a zigzag-like pattern. Molecular dynamic simulations reflected that upon the —SH terminal groups of MPS SAMs were oxidized into $-SO_3H$ groups, the distribution of sulfur atoms in the SAMs arranged in a ordered array that induced the formation of uniform SnO_2 films at the interface. Finally the binding energies of simplified MPS model with different SnO_2 crystal planes were obtained using DFT calculations. The lowest binding energy suggested the existence of strong interactions between the $-SO_3H$ groups of SAMs and the (110) plane of SnO_2, which was due to the structural and electrical match between the $-SO_3H$ group and the unsaturated atoms in the SnO_2 (110) plane.

Combining experimental results with molecular calculations, it is concluded that not only the length of alkyl chain but also the terminal group significantly influence the packing structure of SAMs. The SO_3H-terminated MPS can self-assemble into relatively ordered monolayer that plays a dominant role in adjusting the crystal orientation of the deposited SnO_2 film at the interfaces. These results provide us with a useful route to induce epitaxial growth of metal oxides at the interfaces, which is an attractive point to produce desirable crystal semiconductor films and catalysts.

Acknowledgments

The work described here is sponsored by the NSFC (No. 20576090 and 20676096), the PCSIRT, the Special Funds for Major State Basic Research Program of China (2006CB202500), the Program of Introducing Talents of Discipline to Universities (No. B06006), and the New Century Excellent Talents in the university. We greatly appreciate Dr. Yi Lu, Professor of Chemistry and Biochemistry in University of Illinois, Urbana-Champaign, for his kind modification for this article.

Literature Cited

1. Choi GY, Kang JF, Ulman A, Zurawsky W, Fleischer C. Acid-base interaction in the adhesion between two solid surface. *Langmuir*. 1999;15:8783–8786.
2. Depalma V, Tillman N. Friction and wear of self-assembled trichlorosilane monolayer films on silicon. *Langmuir*. 1989;5:868–872.
3. Keefe MH, Slone RV, Hupp JT, Czaplewski KF, Snurr RQ, Sterm CL. Mesoporous thin film of "molecular squares" as sensors for volatile organic compounds. *Langmuir*. 2000;16:3964–3970.
4. Liu Y, Mills RC, Boncella JM, Schanze KS. Fluorescent polyacetylene thin film sensor for nitroaromatics. *Langmuir*. 2001;17:7452–7455.
5. Sieval AB, Linke R, Zuilhof H, Sudholter EJR. High-quality alkyl monolayers on silicon surfaces. *Adv Mater*. 2000;12:1457–1460.
6. Stewart MP, Buriak JM. Chemical and biological applications of porous silicon technology. *Adv Mater*. 2000;12:859–869.
7. Abdelghani A, Hleli S, Cherif K. Optical and electrochemical characterization of self-assembled octadecyltrichlorosilane monolayer on modified silicon electrode. *Mater Lett*. 2002;56:1064–1068.
8. Strother T, Cai W, Zhao X, Hamers RJ, Smith LM. Synthesis and characterization of DNA-modified silicon (111) surfaces. *J Am Chem Soc*. 2000;122:1205–1209.
9. Shirahata N, Hozumi A, Asakura S, Fuwa A, Sakka Y. Assembly of hydrothermally synthesized tin oxide nanocrystals. *J Vacuum Sci Technol (A)*. 2005;23:731–736.
10. Shirahata N, Masuda Y, Yonezawa T, Koumoto K. Control over film thickness of SnO_2 ultrathin film selectively deposited on a patterned self-assembled monolayer. *Langmuir*. 2002;18:10379–10385.
11. Supothina S, De Guire MR. Characterization of SnO_2 thin films grown from aqueous solutions. *Thin Solid Films*. 2000;371:1–9.
12. Turgeman R, Gershevitz O, Deutsch M, Ocko BM, Gedanken A, Sukenik CN. Crystallization of highly oriented ZnO microrods on carboxylic acid-terminated SAMs. *Chem Mater*. 2005;17:5048–5056.
13. Aizenberg J, Black AJ, Whitesides GM. Oriented growth of calcite controlled by self-assembled monolayers of functionalized alkanethiols supported on gold and silver. *J Am Chem Soc*. 1999;121:4500–4509.
14. Travaille AM, Donners JJJM, Gerritsen JW, Sommerdijk NAJM, Nolte RJM, Kempen H. Aligned growth of calcite crystals on a self-assembled monolayer. *Adv Mater*. 2002;14:492.
15. Travaille AM, Kaptijn L, Verwer P, Hulsken B, Elemans JAAW, Nolte RJM, Kempen H. Highly oriented self-assembled monolayers as templates for epitaxial calcite growth. *J Am Chem Soc*. 2003;125:11571–11577.
16. Shin H, Collins RJ, De Guire MR, Heuer AH, Sukenik CN. Synthesis and characterization of TiO_2 thin films on organic self-assembled monolayers. I. Film formation from aqueous solutions. *J Mater Res*. 1995;10:692–698.
17. Shin H, Collins RJ, De Guire MR, Heuer AH, Sukenik CN. Synthesis and characterization of TiO_2 thin films on organic self-assembled monolayers. II. Film formation via an organometallic route. *J Mater Res*. 1995;10:699–703.

18. Ito E, Konno K, Noh J, Kanai K, Ouchi Y, Seki K, Hara M. Chain length dependence of adsorption structure of COOH-terminated alkanethiol SAMs on Au(111). *Appl Surf Sci*. 2005;244:584–587.
19. Noble-Luginbuhl AR, Nuzzo RG. Assembly and characterization of SAMs formed by the adsorption of alkanethiols on zinc selenide substrates. *Langmuir*. 2001;17:3937–3944.
20. Prathima N, Harini M, Rai N, Chandrashekara RH, Ayappa KG, Sampath S, Biswas SK. Thermal study of accumulation of conformational disorders in the self-assembled monolayers of C8 and C18 alkanethiols on the Au(111) surface. *Langmuir*. 2005;21:2364–2374.
21. Wei BJ, Himmel HJ, Fischer RA, Wöll C. Self-terminated CVD-functionalization of organic self-assembled monolayers (SAMs) with trimethylamine alane (TMAA). *Chem Vapor Deposition*. 1998;4:17–21.
22. Lahiri J, Ostuni E, Whiltesides GM. Patterning ligands on reactive SAMs by microcontact pringting. *Langmuir*. 1999;15:2055–2060.
23. Sieval AB, Hout B, Zuilhof H, Sudholter EJR. Molecular modeling of alkyl monolayers on the Si(111) surface. *Langmuir*. 2000;16:2987–2990.
24. Sieval AB, Hout B, Zuilhof H, Sudholter EJR. Molecular modeling of covalently attached alkyl monolayers on the hydrogen-terminated Si(111) surface. *Langmuir*. 2001;17:2172–2181.
25. Zhang LC, Wesley K, Jiang SY. Molecular simulation study of alkyl monolayers on Si(111). *Langmuir*. 2001;17:6275–6281.
26. Pei Y, Ma J, Jiang YS. Formation mechanisms and packing structures of alkoxyl and alkyl monolayers on Si(111): theoretical studies with quantum chemistry and molecular simulation models. *Langmuir*. 2003;19:7652–7661.
27. Ferrere S, Zaban A, Gregg BA. Dye sensitization of nanocrystalline tin oxide by perylene derivatives. *J Phys Chem B*. 1997;101:4490–4493.
28. Chen FL, Shi Z, Liu ML. Praparation of mesoporous SnO_2-SiO_2 composite as electrodes for lithium batteries. *Chem Commun*. 2000;21:2095–2096.
29. Mattos M, Morales J, Sánchez L. Mechanochemical synthesis of $Sn_{1-x}Mo_xO_2$ anode materials for Li-ion batteries. *J Mater Chem*. 2002;12:2979–2984.
30. Goebbert C, Aegerter MA, Burgard D, Nass R, Schmidt H. Ultrafiltration conducting membranes and coating from redispersable, nanoscaled, crystalline SnO_2: Sb particles. *J Mater Chem*. 1999;9:253–258.
31. Law M, Kind H, Messer B, Kim F, Yang PD. Photochemical sensing of NO_2 with SnO_2 nanoribbon nanosensors at room temperature. *Angew Chem Int Ed Eng*. 2002;41:2405–2408.
32. Wang Y, Jiang X, Xia Y. A solution-phase, precursor route to polycrystalline SnO_2 nanowires that can be used for gas sensing under ambient conditions. *J Am Chem Soc*. 2003;125:16176–16177.
33. Tsukuma K, Akiyama T, Imai H. Liquid phase deposition film of tin oxide. *J Non-Crystalline Solids*. 1997;210:48–54.
34. Supothina S, De Guire MR. Characterization of SnO_2 thin films grown from aqueous solutions. *Thin Solid Films*. 2000;371:1–9.
35. Supothina S, De Guire MR, Heuer AH. Nanocrystalline tin oxide thin films via liqid flow deposition. *J Am Ceramic Society*. 2003;86:2074–2081.
36. Zhang JL, Li W, Zhai Y, Yang H, Wang YP. Growth of SnO_2 thin films on self-assembled layers of the short-chain alkoxysilane. *Appl Surf Sci*. 2005;245:94–101.
37. *Materials Studio 3.0*, Accelrys Software, San Diego, CA.
38. Sun H. COMPASS: an ab initio forcefield optimized for condensed-phase applications—overview with details on alkane and benzene compounds. *J Phys Chem B*. 1998;102:7338–7364.
39. Buriak JM. Organometallic chemistry on silicon and germanium surfaces. *Chem Rev*. 2002;102:1271–1308.
40. Hamers RJ, Wang Y. Atomically-resolved studies of the chemistry and bonding at silicon surfaces. *Chem Rev*. 1996;96:1261–1290.
41. Hess JS, Doren DJJ. Surface electronic excited state on Si(100): structure, energetics, lifetime, and role in chemical reactions. *J Phys Chem B*. 2002;106:8206–8210.
42. Morikawa Y. Adsorption geometries and vibrational modes of C_2H_2 on the Si(001) surface. *Phys Rev B*. 2001;63:033405.
43. Miotto R, Ferraz AC, Srivastava GP. Acetylene adsorption on the Si(001) surface. *Phys Rev B*. 2002;65:075401.
44. Berendsen HJC, Postma JPM, Gunsteren WF, DiNola A, Haak JR. Molecular dynamics with coupling to an external bath. *J Chem Phys*. 1984;81:3684–3690.
45. Perdew JP, Burke K, Ernzerhof M. Generalized gradient approximation made simple. *Phys Rev Lett*. 1996;77:3865–3868.
46. Senkevich JJ, Mitchell CJ, Yang GR, Lu TM. Surface chemistry of mercaptan and growth of pyridine short-chain alkoxy silane molecular layers. *Langmuir*. 2002;18:1587–1594.
47. Stevens MJ. Thoughts on the structure of alkylsilane monolayers. *Langmuir*. 1999;15:2773–2778.
48. Zhang LC, Leng YS, Jiang SY. Tip-based hybrid simulation study of frictional properties of self-assembled monolayers: effects of chain length, terminal group, scan direction, and scan velocity. *Langmuir*. 2003;19:9742–9747.
49. Leng YS, Jiang SY. Atomic indentation and friction of self-assembled monolayers by hybrid molecular simulations. *J Chem Phys*. 2000;113:8800–8806.
50. Lee AY, Ulman A, Myerson AS. Crystallization of amino acids on self-assembled monolayers of rigid thiols on gold. *Langmuir*. 2002;18:5886–5898.
51. Kang JF, Zaccaro J, Ulman A, Myerson A. Nucleation and growth of glycine on self-assemble monolayers on gold. *Langmuir*. 2000;16:3791–3796.
52. Supothina S, De Guire MR, Heuer AH. Nanocrystalline tin oxide thin films via liquid flow deposition. *J Am Ceramic Soc*. 2003;86:2074–2081.
53. Henrich VE, Cox PA. *The Surface Science of Metal Oxides*. Cambridge: Cambridge University Press, 1994:43.

Manuscript received Feb. 5, 2007, and revision received Aug. 1, 2007.